Particle Control for Low-Energy Boron Implantation

CFM: Contamination-Free Manufacturing

Phillip Geissbühler, David Burtner, Charlie Free, Kevin Wenzel, Luke Kim, DaeYoon Kim, BuMin Son
Axcelis Technologies
Phillip.Geissbuhler@axcelis.com

HunKyu Cha, SangHyun Na
SK hynix
HunKyu.Cha@sk.com, SangHyun.Na@sk.com

We present a case study describing how particles added to wafers during dedicated low-energy boron (LEB) implants can be reduced by the implementation of new hardware to reduce the buildup of boron films on beamline components. The new hardware increases the ion beam angle of incidence on beamline component surfaces to enhance self-sputtering of films and significantly reduces the film growth rate on surfaces near the wafer being implanted. This is important because film growth can lead to delamination which is a particle source. Particle adders can reduce device yields.

I. Dedicated Low Energy B+ implants lead to film creation and particles

Axcelis' Purion High Current (Purion HC) implanter uses graphite liners to shield areas of the process chamber from beam-strike. This includes a beam tunnel and liners surrounding dosimetry components in the near wafer environment. Figure 1 shows the presence of boron films on the Purion HC beam tunnel and dose Faraday aperture after running dedicated LEB implants.

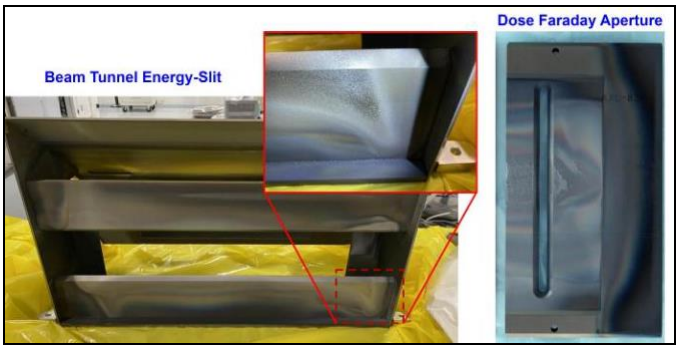

Fig. 1. Boron film accumulation on the Purion HC beam tunnel and dose Faraday aperture after running dedicated low-energy boron.

Implanters that run dedicated LEB have been shown to accumulate 10 to 20µm thick films on beam-facing surfaces after only 10 days of exposure. Figure 2 is a scanning electron microscopy (SEM) image of a cross-section of the dose Faraday aperture of a Purion HC implanter after running dedicated LEB. Both the boron film and the graphite substrate were identified using energy-dispersive x-ray spectroscopy (EDX). The film was measured to be nearly pure boron, not a boron-carbon compound.

The buildup of films when running dedicated boron implants is different than when running mixed species. At normal incidence, LEB beams do not self-sputter well. When running mixed species, heavier ions can sputter off films that develop thereby keeping those surfaces cleaner for a longer period. Once these films grow, they can delaminate and transfer particles, especially large particles (> 300nm), onto the wafer being implanted.

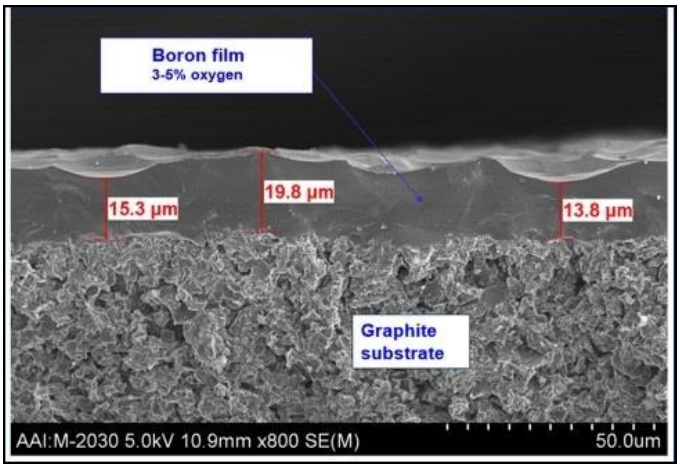

Fig. 2. SEM cross-section of a Purion HC dose Faraday aperture after running dedicated LEB.

We used a KLA SP5 particle counter to generate maps of those wafers that experienced a particle excursion (i.e., when particles ≥ 45nm in size exceeded the particle specification). The maps show a random distribution pointing to a beam-borne source. The SP5 saturates at particle sizes ≥ 500nm so those particles that are larger are labeled as being 500nm. Those same wafers were then run through a KLA eDR7380 for EDX analysis. Figure 3 is a boxplot of all particles seen on a wafer that experienced a particle excursion. Those particles that did not contain boron are in bin (0) and those that did contain boron are in bin (1). Note the large number of saturated boron-containing particles. The median size of each bin is also shown. When comparing the size of defects found on the wafer, those containing boron were significantly larger than non-boron particles.

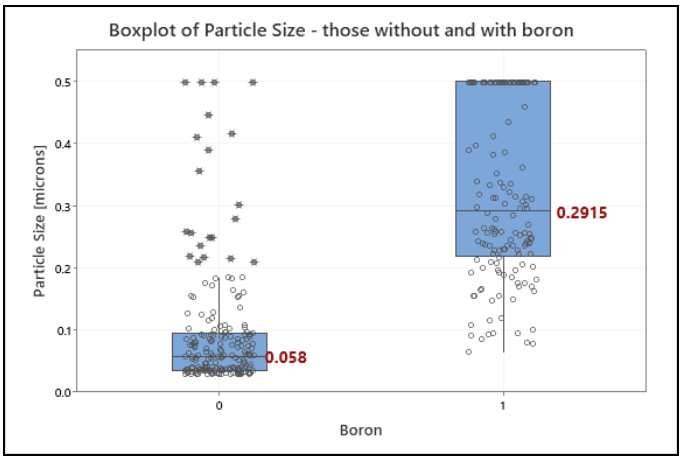

Fig. 3. Sizes of all particles found on a wafer that experienced a particle excursion. Bin (0) particles do not contain boron. Bin (1) particles contain boron. Each bin is labeled with its median size.

Figure 4 is a set of SEM images of large particles (several microns) found on wafers that experienced particle excursions. Those with shape Type 2, which look like delaminated flakes, were the most prevalent (85%).

	Shape Type 1	Shape Type 2	Shape Type 3
SEM		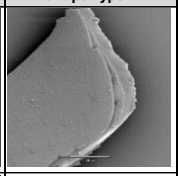	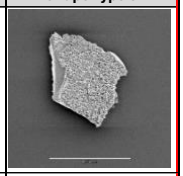
SEM	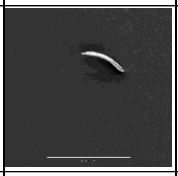	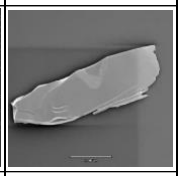	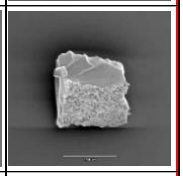
Fraction of Total Number of Particles	3%	85%	12%

Fig. 4. SEM images of particles on wafers that experienced a particle excursion. Particles from 10 wafers were classified as one of three shape types. The fraction of particles of each shape type is shown. Each SEM image includes a 1µm (or 0.5µm bottom right SEM) bar for scale.

Analysis of three flake-shaped particles found on wafers using SEM, EDX, transmission electron microscopy (TEM), and electron energy loss spectroscopy (EELS) is shown in Figure 5. The particles comprise primarily boron. Argon and arsenic were also seen in much lower quantities, as is expected from an implanter dedicated to low-energy boron implants that occasionally runs Ar+ and As+ beams.

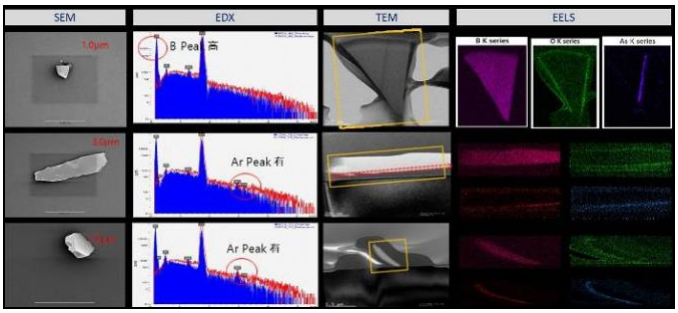

Fig. 5. SEM, EDX, TEM, and EELS analysis of wafer particles

To identify the origin of these particles we analyzed films on the surfaces that come into contact with the beam including the beam tunnel and the front apertures and side shields of the dose Faraday and profiler (Figure 6). The species and relative concentrations of these films matched those of the large particles seen on the wafer.

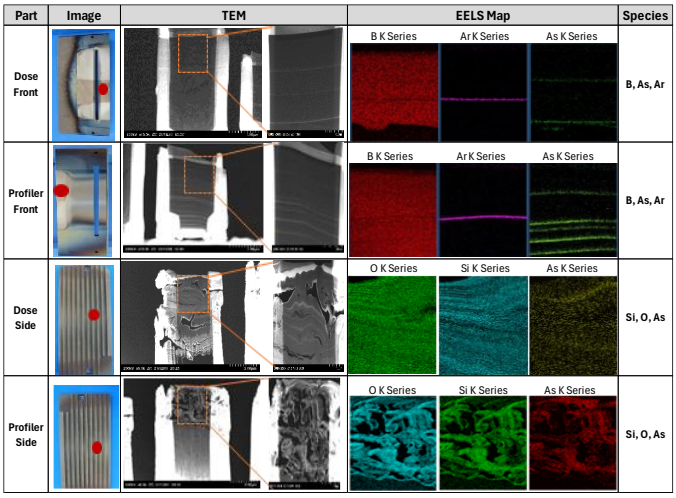

Fig. 6. TEM & EELS analysis of films on Faraday graphite liners

II. Reduction of film formation rate

When the number of particles on the wafer approaches or exceeds the cleanliness specification, the graphite liners are replaced, ideally during periodic preventative maintenance (PM). It is desirable to extend the time between PMs to increase uptime and reduce cost of ownership.

One way to extend time between PMs on tools that run dedicated boron is to slow down the boron film growth rate on replaceable parts. Sputtering films on graphite liners by the ion beam can slow the rate of accumulation depending on its sputter yield S defined as the mean number of atoms removed from the surface of a solid per incident ion. Sputter yield is dependent on several factors: incoming atomic species, energy, and incident angle, as well as target material. An incoming beam with sputter yield $S > 1$ can remove more material than it adds.

Sputter yield Monte Carlo simulations were conducted of B+ impinging on a boron film and P+ impinging on a phosphorus film using the SRIM software package [1]. Figure 7 shows the geometry used in the sputtering simulations. A beam traveling directly into (i.e., normal to) the graphite surface is defined as having 0° angle of incidence. The films being sputtered are located on the exposed graphite surface.

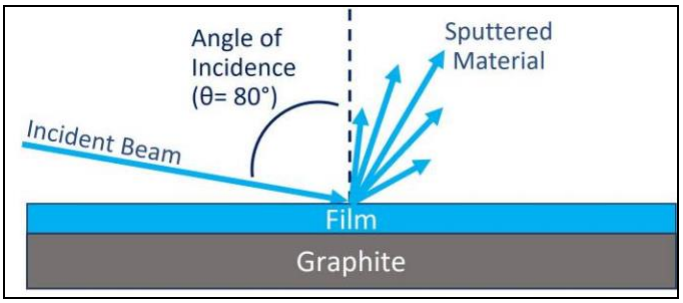

Fig. 7. Geometry used in the sputtering models of films on graphite

Figure 8 is a graph of the sputter yield simulations. In the case of B+ 3keV, the sputter yield S < 1 at normal incidence and increases with incidence angle, peaking at ~80°, before dropping off again. In contrast, P+ 3keV impinging on a phosphorus film has S > 1 at normal incidence and increases with incidence angle.

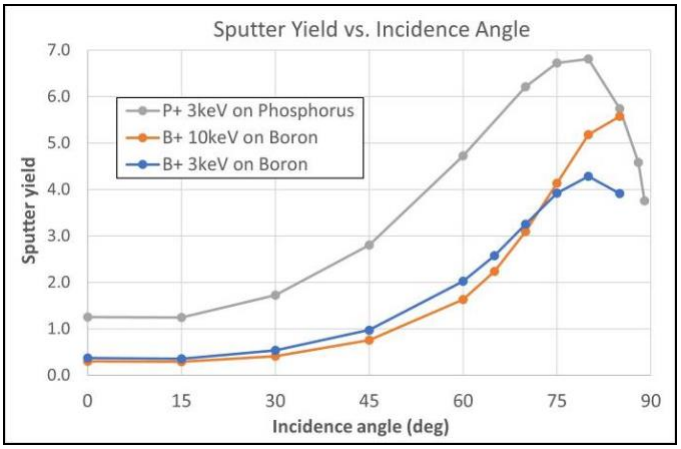

Fig. 8. Sputter yield of B+ on Boron and P+ on Phosphorus Films

III. Description of Sputtering Model of Serrated Graphite

Surfaces that experience glancing angle incidence with the beam will remain clean by the beam self-sputtering off films from the surface. However, surfaces that are normal to a LEB beam will experience sputter yields S < 1 and therefore films will grow, eventually delaminate, and become a particle source. One way to increase self-sputtering is to add serrations to those surfaces that are normal to the beam. Serrations can increase the sputter yield by increasing the angle of incidence, but some of the sputtered material will be redeposited onto the other side of the structure (Figure 9). Note that in this geometry, the angle of incidence (θ) and the serration angle are the same.

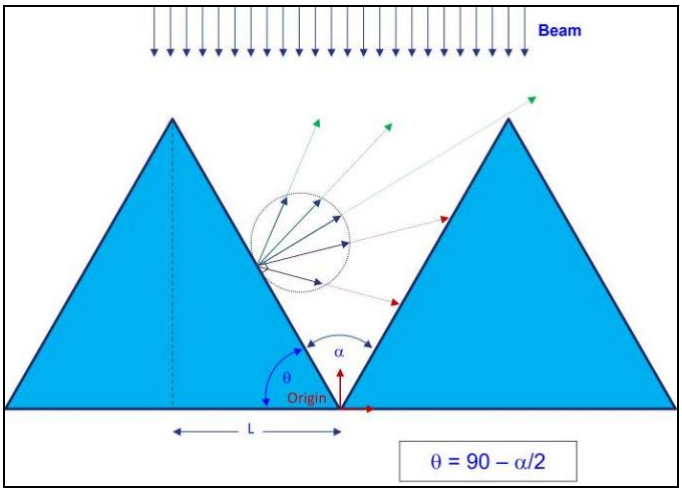

Fig. 9. Geometry of serrated graphite (shown in cross-section) used in our sputtering model. The ion beam (in the vertical direction) is impinging on the graphite surface (only 2 of the many serrations are shown).

We modelled the sputtering of serrated graphite to optimize the serration angle for minimal film deposition. The sputter plume can be modelled in a few different ways: 1) equally distributed through a range of angles, 2) a cosine function, or 3) a more complicated differential angular yield. No sources could be found in the literature of differential angular sputtering of boron by boron. However there is literature on the sputtering of graphite [2] and of low energy light ion sputtering [3]. To first order, the sputter plume can be approximated to have a cosine distribution although, for some species and target combinations, the sputter yield at high incidence angles mentioned in [2 & 3] do not follow a pure cosine distribution. Our model used a sputter plume with a cosine distribution and the following equations:

Current density J = ROI * X*Y*cos(θ)

Film growth rate = $J*m_B/(e*\rho_B)*\cos(\theta)$ ~1.6 μm/day *cos(θ)

Etch rate = $J*m_B/(e*\rho_B)*S(\theta)*\cos(\theta)$

with the following parameters:

L = 1 mm (serration half-width); θ = serration angle

X*Y= cross-sectional area of beam

ROI = 12mA (beam current in the region of interest)

e = electron charge; ρ_B = boron density; m_B = boron mass

S(θ) = sputter yield in atoms/ion

Figure 10 shows the results of modelling boron film growth (>0) or etching (<0) vs. serration angle (θ) assuming a sputter plume with a cosine distribution.

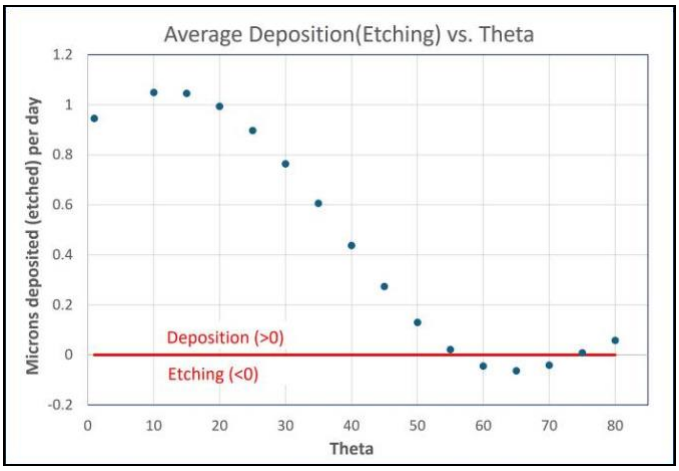

Fig 10. Average boron deposition (>0) or etching (<0) vs. serration angle (θ)

The model predicts that a serration angle θ=65° will maximize the average removal (i.e., etching) of films. Sputtered atoms are biased towards higher angle than normal to surfaces. This distributes more redeposited material to the bottom of the serration valleys. Although the average removal of films is maximized at θ=65°, the model predicts that film growth would still accumulate at the bottom of the valley and the maximum deposition seen on the serrated side walls will continue to fall off with higher angle of incidence θ (Figure 11). This supports testing parts with serrations that are greater than 65°.

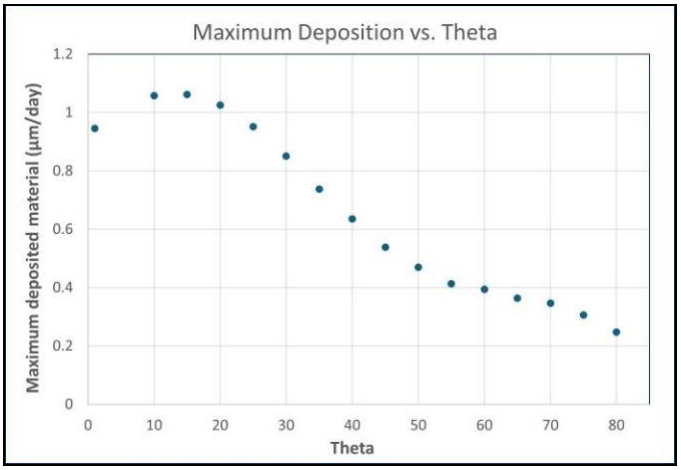

Fig 11. Maximum boron deposition vs. serration angle (θ)

IV. Description of the hardware and modifications

The dose Faraday and beam tunnel apertures have faces normal to the beam and in proximity to the wafer. These beam-facing surfaces were redesigned with serrations to increase the beam's angle of incidence to increase sputter yield and thereby reduce the rate of film buildup [4]. One set has serrations whose surfaces have a high angle of incidence of 60° (HA60) with respect to the beam and a second set with a higher angle of incidence of 75° (HA75). Figure 12 shows both the 60° and 75° serrations of the dose Faraday aperture. Figure 13 shows the redesigned components: the beam tunnel's energy-slit and exit apertures and one of the two dose Faraday apertures.

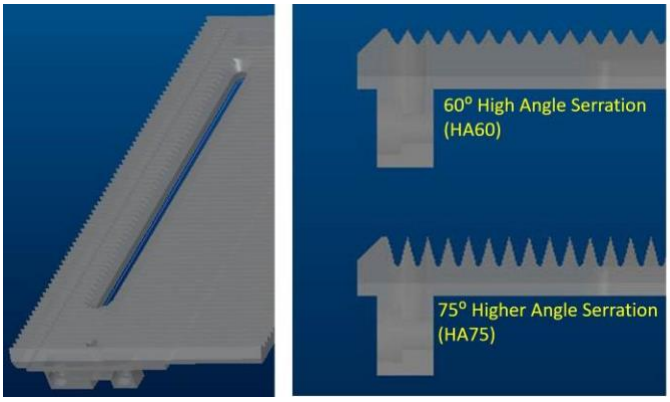

Fig. 12. Cross-sections of Dose Faraday apertures with 60° & 75° serrations

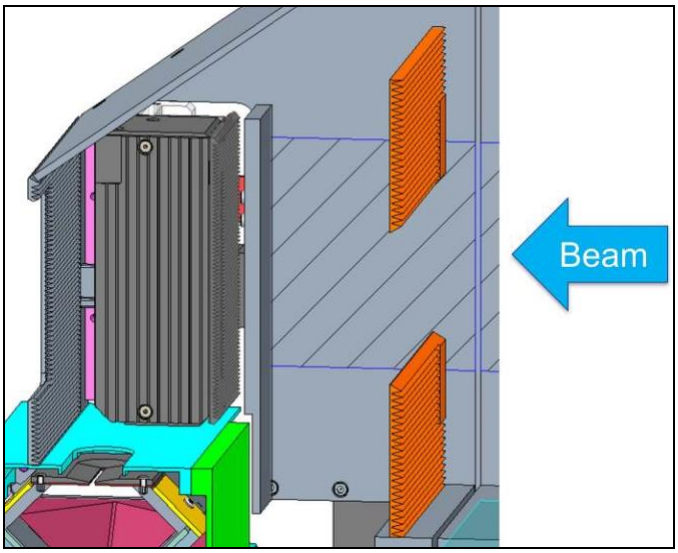

Fig 13. E-slit, Beam Tunnel Exit, and one of the two Dose Faraday Apertures with 75° serrations

V. Results

Daily particle monitoring at SK hynix prior to and after installing the HA60 serrated dose Faraday and beam tunnel apertures are shown in Figure 14. For the 89 days prior to installing the HA60 serrated graphite, particle compliance was 85%. For the 78-day period after installing the HA60 graphite, compliance was 91%, a 6% improvement.

Fig. 14. Daily particle monitors pre- and post-install of HA60 serrated graphite. Shown are adders ≥ 45 nm in size.

In 2024 the HA60 dose Faraday and beam tunnel apertures were replaced with the higher angle of incidence graphite (HA75). Figures 15 & 16 are a set of box plots in which the particle data are binned to include all data between consecutive PMs. The serrated graphite was replaced after each PM. Duration between each of the first 5 PMs shown was between 17 and 21 days. When the HA75 graphite was installed, particle adders remained in spec with 100% compliance so the period was extended to 36 days.

Fig. 15. Particle adders >21nm in size binned for each period between consecutive PMs using HA60 and HA75 components

Fig. 16. Particle adders >150nm in size binned for each period between consecutive PMs using HA60 and HA75 components.

Because of the superior particle performance, the HA75 dose Faraday and beam tunnel apertures were left in the implanter for a total of 4 PM cycles and then removed for inspection. Figure 17 is a comparison of the 60° serration dose Faraday apertures after 1 PM cycle (~20 days) with the 75° serration dose Faraday apertures after 4 PM cycles (~80 days). The light gray film seen on the 60° apertures is significantly thicker than that on the 75° apertures.

Fig. 17. Photographs of serrated dose Faraday apertures removed from a Purion HC implanter running dedicated LEB. The high angle serration (60°) apertures ran for ~20 days, and the higher angle (75°) serration apertures ran for ~80 days.

VI. Conclusion

Surfaces that see direct beam-strike of low-energy boron develop boron films. Serrations added to those surfaces increase the ion beam angle of incidence and thereby enhance the sputtering of boron films that develop. This self-cleaning mechanism slows down the rate of film buildup and thereby increases the duration before films delaminate. By modelling the sputtering behavior of these serrated graphite surfaces we optimized the serration angle to reduce the number of particles impinging on implanted wafers. This has not only improved wafer yield, but also extended the time between PMs which thereby increases uptime and reduces the cost of ownership.

REFERENCES

[1] J. F. Ziegler, M. D. Ziegler, and J. P Biersack, “SRIM – The stopping and range of ions in matter (2010)”, Nucl. Instrum. And Methods in Phys Research Sec. B: Beam Interactions with Mater. And Atoms, vol. 268, no. 11 – 12, pp. 1818 – 1823, June 2010.

[2] Williams, et al., “Differential Sputtering Behavior of Pyrolytic Graphite and Carbon-Carbon Composite Under Xenon Bombardment”, p.3788, AIAA-2004

[3] Roth, Bohdansky, and Ottenberger, “Data on Low Energy Light Ion Sputtering”, Max Planck Institute für Plasmaphysik, 1979

[4] Burtner D., Bassom N., “High incidence angle graphite for particle control with dedicated low sputter yield ion beam”, US Patent Application No. 2023/0235449 A1 (27 July 2023)